Effects of stacking variations on the lattice dynamics of InAs nanowires

N. G. Hörmann,[1] I. Zardo,[1,2] S. Hertenberger,[1] S. Funk,[1,2] S. Bolte,[1,3] M. Döblinger,[3] G. Koblmüller,[1] and G. Abstreiter[1,2]
[1]*Walter Schottky Institut and Physik Department, Technische Universität München, am Coulombwall 4, D-85748 Garching, Germany*
[2]*Institute for Advanced Study, Technische Universität München, Lichtenbergstraße 2 a, D-85748 Garching, Germany*
[3]*Department of Chemistry, Ludwig-Maximilians-Universität München, D-81377 Munich, Germany*
(Received 27 July 2011; published 4 October 2011)

The optical phonon properties of single InAs nanowires and their relation to the crystal structure are studied by means of Raman spectroscopy. The nanowires were grown by molecular beam epitaxy on Si (111) without foreign catalyst and exhibit variations in the stacking sequence with wurtzite and zincblende inclusions. Specific new features, such as a TO frequency shift and selection rules different from bulk InAs, are observed. Further polarization-dependent measurements reveal the existence of four individual peaks in the optical phonon energy range of InAs. By performing a full azimuthal-dependence analysis of the Raman scattering intensity, the individual symmetry behavior of these peaks could be determined, namely the B_1^H, E_2^H, TO ($A_1 + E_1$), and LO (A_1). The B_1^H and E_2^H modes are assigned to wurtzite-type modes.

DOI: 10.1103/PhysRevB.84.155301 PACS number(s): 63.22.Gh, 81.07.Gf, 78.30.Fs, 61.46.Km

I. INTRODUCTION

In recent years, semiconductor nanowires (NWs) have gained increased attention due to their unique geometry and largely altered physical properties as compared to bulk material. In this context, several advanced technological applications have been proposed and demonstrated for a wide range of both elemental and compound semiconductor NWs.[1–5] Particularly promising is the possible integration of III-V semiconductors on Si and, thus, the compatibility with standard CMOS technology.[6–10] Although low-defect density NWs have been reported, many nanowire material systems suffer from various types of planar defects, predominantly rotational twins and twinning superlattices,[11] alternating zincblende (ZB)/wurtzite (WZ) polytypes,[12] as well as point defects.[13] Raman spectroscopy is a versatile technique to characterize materials in an effective and nondestructive way. Phonon energies, scattering cross sections, and symmetry properties of optical phonons are determined by analyzing inelastically scattered light, providing information about the crystal structure and composition, the electronic properties, electron-phonon, and phonon-phonon interactions.[14] Several Raman scattering studies of NWs have been published, where various new effects have to be considered such as significant heating,[15,16] phonon confinement,[17–19] and the *antenna effect*,[20–23] due to the dielectric mismatch between the NW and its surrounding. These effects can alter phonon energies and the observed selection rules. Furthermore, few experiments so far consider the effects of zincblende/wurtzite polytypes and stacking disorder in NWs on the Raman selection rules.[21,24–27] Lattice disorder leads to a relaxation of momentum conservation and non-zone-center phonons contribute to the scattering processes. In this work, InAs NWs have been studied in detail by Raman spectroscopy. The InAs nanowires exhibit large regions with stacking disorder and crystalline domains mainly of wurtzite and partly zincblende structure.

II. EXPERIMENTAL DETAILS

The investigated InAs NWs were grown by solid-source molecular beam epitaxy (MBE) on Si(111), utilizing an ultrathin amorphous SiO_x layer, which serves as a nucleation mask layer for catalyst-free NW growth.[8] The InAs NWs investigated here were from a characteristic sample grown for 8 hrs under a fixed-growth temperature of 460 °C and an As/In ratio of 6.3. Since the NWs were grown in a spatially uncorrelated (i.e., non-site-selective) method, significant diameter (d) and length (l) variation was obtained with values of $d \approx$ 90–240 nm and $l \approx 3.5 \pm 1$ μm, as determined from cross-section scanning electron micrographs in free-standing NW geometry. The NWs exhibit a hexagonal cross-section, as determined by scanning electron microscopy. Further growth details and analysis of the underlying growth mechanism are reported elsewhere.[8,9,28] The epitaxial relationship between the InAs NWs and Si (111) substrate and the predominant crystal structure of these NWs were analyzed by x-ray diffraction (XRD) and transmission electron microscopy (TEM) (Fig. 1). The out-of-plane symmetric XRD 2θ-ω scan shown in Fig. 1(a), which was obtained from the as-grown NWs, indicates that they were grown epitaxially on the Si substrate. Beside the 111 reflection of Si at 28.4°, another asymmetric or split reflection at 25.3° representing variations in the atomic distances in the layered stacking of InAs[29] was observed [Fig. 1(b)]. Electron diffraction patterns of single wires from the same sample indicate a structure based on WZ with a major contribution of stacking disorder along the growth direction. An example is shown in Fig. 1(c). The high-resolution transmission electron microscopy (HRTEM) study, however, shows also small domains with ZB structure besides the regions with WZ structure and disordered regions [Fig. 1(d)].

NWs were transferred by sonication in isopropanol and subsequent dropcasting on a prepatterned SiO_2(200 nm)/Si wafer piece to allow polarization-dependent Raman measurements on single wires. The markers facilitate the identification of individual NWs on the substrate. Prior to the Raman investigations, atomic force microscopy (AFM) measurements were performed in order to determine the NW shape, diameter, and length after transfer. The experimental results presented here were obtained on six individual NWs selected in a diameter range from 90 to 240 nm and lengths between 1.3 and 2.8 μm. Raman investigations have been performed in

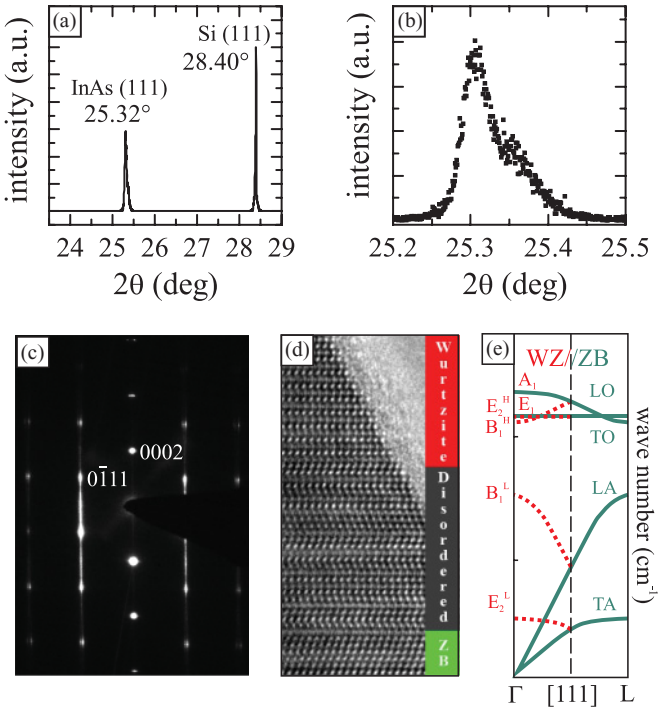

FIG. 1. (Color online) (a) X-ray diffraction scan of a selected InAs nanowire array sample, confirming the epitaxial relationship between InAs(111) and Si(111) substrate. (b) High-resolution diffraction profile in the vicinity of the main InAs diffraction peak, evidencing an elongated reflection due to slightly different atomic distances within the layered stacking of InAs. An electron diffraction pattern of a single wire is shown in (c). All reflections in the diffraction pattern can be indexed according to a wurtzite structure in [10-10] zone axis. The diffuse streaks along the growth direction indicate stacking disorder. A HRTEM image of the same wire in the same orientation is shown in (d). In addition to regions with WZ structure and regions with disordered stacking, a small domain with ZB structure is also visible. (e) Approximated phonon dispersion in InAs wurtzite [0001] (dotted lines) obtained by backfolding the InAs zincblende phonon dispersion along [111] (solid lines). Additional zone center modes appear in the WZ structure. The ZB dispersion is taken from Ref. 30.

a μ-Raman setup in backscattering geometry under ambient conditions, using the 514.5-nm line of an Ar^+-laser or the 647.1-nm line of a Kr^+-laser as excitation and collecting the scattered light by a XY Dilor triple spectrometer equipped with a multichannel Si charge couple device detector. All measurements were performed with a 100× microscope objective (NA = 0.95), resulting in a spot diameter of around 550 and 740 nm for the two different excitation wavelengths and a power density of about 85 kW/cm^2. The sample is placed on a piezo-controlled translational stage with rotational platform, which enables positioning of a single NW with an accuracy of about 10 nm and 1°. Polarizers and half wavelength plates in the beamline allow the selection of polarization of incident and scattered light, as explained in Ref. 21.

III. THEORETICAL CONSIDERATIONS

The investigated NWs exhibit regions with locally ZB and WZ lattice structure, which are stacked along the growth direction [111] of the nanowire [see Figs. 1(c) and 1(d)]. ZB has two atoms per primitive unit cell and T_d^2 symmetry and WZ has four atoms per primitive unit cell and C_{6v}^4 symmetry. Furthermore, the size of the primitive unit cell of WZ is twice as large in [0001] direction as that of ZB [111].[31] Accordingly, the two structures differ in the zone-center phonon modes, which can be probed by Raman spectroscopy. It is possible to estimate the unknown WZ InAs phonon dispersion by backfolding the phonon branches of ZB InAs along [111], as depicted in Fig. 1(e). This simple Brillouin zone-folding procedure is in good agreement with first principle calculations for WZ InAs.[32] The resulting zone-center phonon modes and estimated frequencies are tabulated in Table I. The respective nomenclature indicates the symmetry behavior. To the best of our knowledge, experimental results on energy and symmetry of the individual phonon modes of WZ InAs have not been reported yet in literature.

TABLE I. Phonon frequencies of zincblende InAs at the Γ and L points, which serve as an estimation for the corresponding mode frequencies in wurtzite InAs.

ZB mode	Frequency (cm^{-1})[a]	Corresponding WZ mode
LO(Γ)	238.6	LO (A_1, E_1)
TO(Γ)	217.3	TO (A_1, E_1)
TO(L)	214–215	E_2^H
LO(L)	201–209	B_1^H
LA(L)	139–143	B_1^L
TA(L)	44–50	E_2^L

[a]Taken from Ref. 30.

The scattering intensity I of Raman-active phonons depends, among other things, on the crystal orientation and light polarization. It provides information on the symmetry of the phonon mode and can be described by a tensor operation:[33]

$$I \propto [\mathbf{e_i} R(\xi) \mathbf{e_s}]^2, \quad (1)$$

where $\mathbf{e_i}$ and $\mathbf{e_s}$ are the polarizations of incident and scattered light and $R(\xi)$ is the Raman tensor of the probed phonon for polarization ξ as tabulated in standard textbooks[14] for the conventional principal axes, as defined in Ref. 34. Depending on the geometry, appropriate transformations according to the properties of a third rank tensor must be applied to $R(\xi)$ (see, e.g., Ref. 33). The optical phonon modes of ZB have T_2 symmetry and are split into LO and TO. In a crystal with WZ structure, the Raman active phonons have A_1, E_1, and E_2 symmetry. If atomic force constants are nonisotropic, LO and TO modes split into A_1 and E_1 components, as E modes correspond to atomic displacements perpendicular to the [0001] direction and A_1 modes along it.[35]

Heterostructures and superlattices exhibit an altered symmetry in one direction, which modifies Raman selection rules.[36] Similar effects can be expected in NWs with twinning, stacking faults, polytype heterostructures, uniaxial strain, and planar defects, as in our case. Furthermore, defects contribute to a relaxation of momentum conservation, which means that not only zone center modes but also modes with finite $\mathbf{q}$ can take part in the scattering process. Disorder can be accounted for within the phonon confinement model (PCM), where a Gaussian shaped distribution of phonon states of the

perfect crystal around $\mathbf{q} = 0$ is assumed to contribute to the scattering profiles.[37] The typical width of this Gaussian is connected to the correlation length L, the average distance of two defects. Considering the typical dispersion of LO and TO in diamond- and zincblende-type crystals an asymmetric broadening and downshift of both LO and TO is expected.[18] Due to the contributing states next to the BZ center, no distinct new features are predicted. In another model, proposed by Nakashima *et al.*,[38,39] which seems more appropriate for stacking faults and WZ/ZB twinning, typical stacking-fault distances L give rise to contributions from phonons from the whole BZ with a maximum at $\mathbf{q} \neq 0$, which scales with $1/L$. This model assumes short-range order and predicts more features in the Raman spectra than the PCM due to increased contribution from states near the BZ boundaries, where the phonon density of states is large.[40]

IV. RESULTS AND DISCUSSION

Raman measurements have been performed in backscattering from the (111) surface of a bulk InAs single crystal as reference, where scattering by LO and TO phonon modes is allowed, and on single InAs NWs. The general measurement geometry for a transferred NW is depicted in Fig. 2(a). The coordinate system $\mathbf{x}'$,$\mathbf{y}'$,$\mathbf{z}'$ is chosen according to the nanowire geometry and the corresponding cubic crystallographic directions. Backscattering occurs from a NW side facet along the direction $\mathbf{x}' = [1\bar{1}0]$. The coordinates $\mathbf{y}'$ and $\mathbf{z}'$ are chosen perpendicular and parallel to the NW axis, respectively. It should be pointed out here that LO scattering is forbidden in this scattering configuration.

Representative Raman spectra obtained from such measurements are depicted in Fig. 2(b). For bulk InAs (111), TO and LO are found at 217.2 and 237.9 cm^{-1}, respectively, as expected.[30] The Raman spectrum of the InAs NW was collected with incident light polarization perpendicular to the NW axis and no polarization selection for the scattered light.

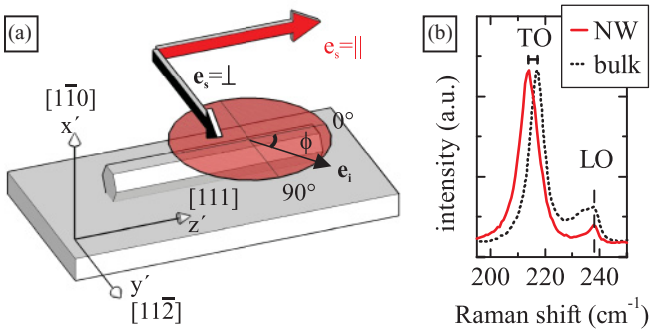

FIG. 2. (Color online) (a) Illustration of the scattering geometry for Raman measurements on transferred InAs nanowires. The Cartesian coordinate system is chosen according to the nanowire crystal directions and geometry, with $\mathbf{z}'$ and $\mathbf{y}'$ parallel and perpendicular to the nanowire axis, respectively. Incident and scattered light polarizations $\mathbf{e_i}$ and $\mathbf{e_s}$ lie in the plane perpendicular to the backscattering direction $\mathbf{x}'$. (b) Representative Raman spectra of bulk InAs and a single InAs nanowire. The TO peak of the InAs nanowire is found at significantly lower Raman shift, whereas the LO coincides well with the bulk value.

A strong peak close to the TO mode of the bulk crystal is dominating the spectrum. However, in addition, the LO mode is also visible at around 238 cm^{-1}. The finite LO intensity is probably related to disorder and to an imperfect scattering geometry (i.e., scattered light is also collected from the side facets, which are not perpendicular to the incident light). Interestingly, the TO mode of the InAs NWs exhibits a downshift of about 3–4 cm^{-1} compared to the TO mode in bulk ZB InAs. Along with the downshift, a clear increase of the full width at half maximum (FWHM) to 8 cm^{-1} is observed. Downshifts of both LO and TO modes can be explained, for example, by the formerly discussed PCM by $\mathbf{q} \neq 0$ scattering due to defects or disorder.[24,25] Also, local heating leads to downshift and broadening and it is a well-known effect occurring in Raman spectroscopy from single nanowires.[16,41] In our case, no significant change could be observed for the InAs LO frequency, which makes both explanations unlikely. Especially InAs would request a pronounced LO shift for disorder-induced scattering due to the large dispersion compared to the very flat dispersion of the TO branch [see Fig. 1(e)]. Furthermore, a power-dependent series of measurements was performed and no significant heating effect was observed under conditions used in this study. A similar downshift of the TO in InAs nanowires for the very same probing laser wavelength has been reported in Ref. 42, however, without closer examination of its origin. It should be mentioned that we observe the downshift of the TO-mode also in ensemble measurements on the as-grown nanowire samples.

In order to get more information, polarization-dependent Raman measurements have been performed on several positions on six individual NWs. Incident and scattered light polarizations were selected either parallel or perpendicular to the NW axis. The obtained Raman spectra are labeled according to the Porto notation $\mathbf{k_i}(\mathbf{e_i}\mathbf{e_s})\mathbf{k_s}$ in the coordinate system as defined in Fig. 2(a), where $\mathbf{k_i}$ and $\mathbf{k_s}$ are the directions of the incident and scattered light and $\mathbf{e_i}$ and $\mathbf{e_s}$ the respective polarizations. For the two main *polarized* scattering configurations, where incident and scattered light is polarized either perpendicular—$\bar{\mathbf{x}}'(\mathbf{y}'\mathbf{y}')\mathbf{x}'$—or along—$\bar{\mathbf{x}}'(\mathbf{z}'\mathbf{z}')\mathbf{x}'$—the NW axis, measurements have been performed with a laser wavelength of 514.5 and 647.1 nm. Representative results are depicted in Fig. 3.

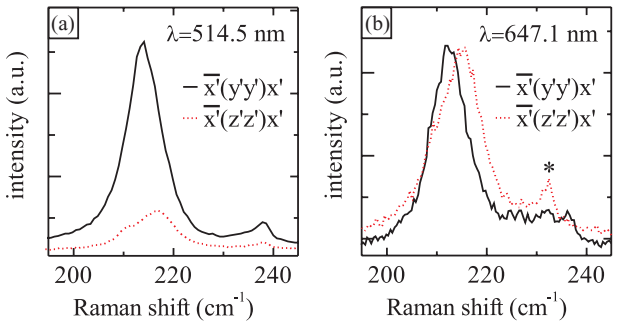

FIG. 3. (Color online) Raman spectra of a InAs NW of 150 nm diameter for the two main polarized scattering configurations collected with (a) 514.5 nm and (b) 647.1 nm excitation wavelength. The peak in (b) labeled with an asterisk is a plasma line of the Kr^+ laser.

Here, the intensity of the $\bar{\mathbf{x}}'(\mathbf{y}'\mathbf{y}')\mathbf{x}'$ configurations of the two excitation wavelengths have been normalized, while the relative intensity of the $\bar{\mathbf{x}}'(\mathbf{z}'\mathbf{z}')\mathbf{x}'$ configurations with respect to the other has been maintained. For the 514.5-nm excitation wavelength, the scattering intensity is enhanced. Furthermore, a relative enhancement of scattering under the $\bar{\mathbf{x}}'(\mathbf{y}'\mathbf{y}')\mathbf{x}'$ configuration with respect to the $\bar{\mathbf{x}}'(\mathbf{z}'\mathbf{z}')\mathbf{x}'$ configuration is observed [Fig. 3(a)]. From standard zincblende selection rules, however, the intensity ratio should be $\frac{3}{4}$, instead of ≈ 5, as observed for the 514.5-nm excitation wavelength. Such an enhancement is not observed for 647.1 nm [Fig. 3(b)].

A deviation from selection rules can be related to the so-called *antenna effect*, which arises due to polarization-dependent coupling efficiencies of light to a nanowire.[20] Depending on the dielectric properties, nanowire diameter, laser wavelength, and especially polarization, light couples with different efficiency to fundamental cavity modes of the waveguide-like nanowire and thus influences the Raman scattering cross section.[43] Such effects are well understood and can be included in the expected polar behavior of the scattering cross section by introducing matrices to Eq. (1), which account for the polarization dependence of in- and out-coupling of light.[23] In order to take these effects into account, simulations have been performed with MEEP,[44] a finite-differences Maxwell equation solver, predicting the polarization-dependent coupling efficiency of the 514.5-nm light to the InAs NW. Dielectric properties were taken from Ref. 45. Due to the E_0 gap of InAs of only 0.34 eV, strong absorption occurs in InAs in the visible. This strongly reduces the strength of the *antenna effect* as no standing waves can form inside the nanowire. The simulations predict no effect for a NW with 150-nm diameter, such as investigated in Fig. 3(a), i.e., both light polarizations parallel and perpendicular to the NW axis couple equally strong to the nanowire. Furthermore, only weak variations of the polarization dependence have been observed in the investigated diameter range of 90–240 nm, which excludes major contributions of the *antenna effect* as it would necessarily scale with nd/λ, where n is the refractive index, d the NW diameter, and λ the excitation wavelength.

Thus we conclude that the observed enhancement for the 514.5-nm excitation is a resonance effect due to the proximity to the E_1 gap in InAs.[46] Furthermore, a recent resonant Raman study on WZ InAs nanowires shows a redshift of the E_1 energy transition of about 100 meV from the bulk value.[47] It is worth to note here, that the enhancement does not occur for both polarizations to the same extent (see Fig. 3 and Ref. 47). We are currently performing further detailed investigations in order to clarify the origin of this resonance effect. Apart from this, Fig. 3 reveals that the TO peak position depends on the polarization. This shift is observed for both wavelengths. We have performed a detailed polarization-dependent study with the 514.5-nm laser line, where the signal to noise ratio is increased due to the resonance enhancement. Also the *depolarized* scattering configurations were recorded. Representative, normalized spectra are depicted in Figs. 4(a)–4(d) as gray squares.

The minimum number of Lorentzians, to fit consistently the TO lineshape, is two for all investigated wires. Furthermore, in the $\bar{\mathbf{x}}'(\mathbf{z}'\mathbf{z}')\mathbf{x}'$ configuration [Fig. 4(b)], a clear shoulder at around 210 cm^{-1} occurs, which is accounted for by a third Lorentzian. Representative multiple Lorentzian

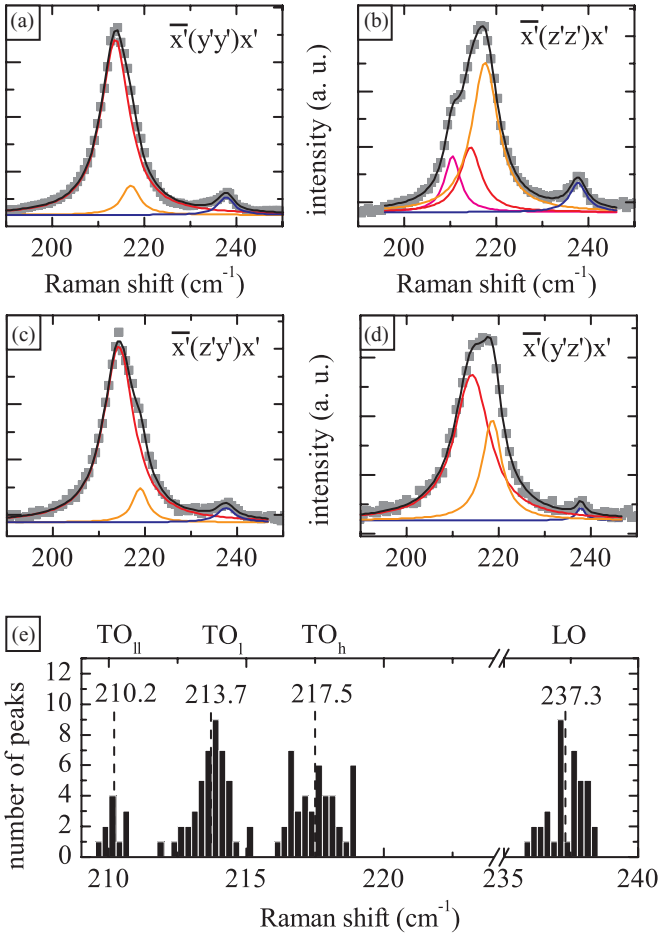

FIG. 4. (Color online) (a)–(d) Representative, polarization-dependent Raman spectra (gray squares) of a 150-nm-thick InAs nanowire. The decomposition into individual Lorentzian contributions is given by the solid lines. (e) Histogram of peak frequencies obtained from Lorentzian fits as in (a)–(d) for the four scattering geometries and for measurements on several positions on six individual nanowires. Four clearly separated peaks arise.

decompositions in the 190–250 cm^{-1} frequency range are depicted in Figs. 4(a)–4(d) as solid lines. The obtained optical phonon peak frequencies for all measurements on all wires are summarized in the histogram of Fig. 4(e). Specifically, a total number of 11 positions on the six wires have been investigated under the four main polarization configurations. The independent contributions are clearly separated and are named according to their relative position: the LO at 237.3 cm^{-1}, the high-lying TO_h at 217.5 cm^{-1}, the low-lying TO_l at 213.7 cm^{-1}, and the shoulder TO_{ll} at the even lower frequency of 210.2 cm^{-1}. The TO_l dominates the signal for the $\bar{\mathbf{x}}'(\mathbf{y}'\mathbf{y}')\mathbf{x}'$ configuration, the TO_h dominates for $\bar{\mathbf{x}}'(\mathbf{z}'\mathbf{z}')\mathbf{x}'$, and in the *depolarized* spectra, both modes are visible. Instead, the TO_{ll} is visible only under the $\bar{\mathbf{x}}'(\mathbf{z}'\mathbf{z}')\mathbf{x}'$ configuration. The frequency of the TO_h mode corresponds to the bulk zincblende TO. The frequencies of the TO_l and of the TO_{ll} modes exhibit rather good correspondence with the frequencies of the ZB zone edge modes in [111] direction (see Table I). Their appearance can either be due to the discussed BZ backfolding mechanism in wurtzite or the stacking-fault-induced mapping

of the density of states as proposed by Nakashima. As the measured spectra, however, are well accounted for by only two (three) Lorentzian peaks, we believe that these lower-lying modes are due to the predominant wurtzite structure of the nanowires. The stacking-fault- or defect-induced mapping of the density of states would result in more complex and asymmetric lineshapes.

In order to confirm the wurtzite-related origin, full azimuthal-dependent measurements have been performed on two nanowires. The polarization of scattered light $\mathbf{e_s}$ was kept fixed either parallel or perpendicular to the NW axis. The incident light polarization $\mathbf{e_i}$ was rotated stepwise, with the angle ϕ between incident light polarization and the nanowire axis [see Fig. 2(a)]. The step size was $10 \pm 2^\circ$. Afterwards multiple peak fits were applied to follow the individual azimuthal dependence of each peak and compare the results to theoretical expectations. Due to the strong overlap of the peaks, a special fitting procedure was applied, by first determining the FWHM for each peak TO_h, TO_l, and TO_{ll} individually. This was achieved by summing up the squared fit errors of several measurements, for different, fixed parameter sets of FWHM. Then the optimum set of FWHM is determined by the minimum of this combined error. After that, the FWHM of each peak was kept fixed, as they are not expected to depend on polarization, and fits were performed to all spectra. The obtained polar behavior of each peak is depicted for one investigated wire in Figs. 5(a)–5(d). Clearly, the different peaks show different polar behavior. Corresponding polar behavior of appropriate wurtzite-type Raman tensors is depicted in Figs. 5(e)–5(h).

As mentioned earlier, LO and TO can be A_1-E_1 split in WZ. In our case, the polar behavior of the LO is well represented by A_1 symmetry [see Figs. 5(a) and 5(e)]. The comparison of TO_h [Fig. 5(b)] and TO_l [Fig. 5(c)] behavior shows three major differences: (i) TO_h does not go to zero for the crossed configurations; the pattern resembles open dipoles of similar intensity. (ii) TO_l approaches zero in the crossed polarizations and the component of the scattered light polarized parallel to the NW axis is nearly missing [circles in Fig. 5(c)]. (iii) The maximum scattering intensity of TO_l is much stronger than that of TO_h.

TO_h is well described by TO behavior, adding up A_1 and E_1 contributions (see Figs. 5(b) and 5(f)]. In principle, the A_1(TO) component is visible under the configuration $\bar{\mathbf{x}}'(\mathbf{z}'\mathbf{z}')\mathbf{x}'$, which corresponds to the dot at 0° in Fig. 5(b), the E_1(TO) contribution under $\bar{\mathbf{x}}'(\mathbf{y}'\mathbf{z}')\mathbf{x}'$, which corresponds to the dot at 90°. Due to the small A_1-E_1 splitting, it is not possible to separate both contributions and, therefore, the Raman tensors of both modes contribute to the TO_h behavior. Under the $\bar{\mathbf{x}}'(\mathbf{z}'\mathbf{z}')\mathbf{x}'$ configuration, the contribution of the zincblende TO mode to this peak cannot be excluded, though the relative intensity of the single contributions is here most probably affected by the observed resonant behavior. The weak scattering component for *polarized* light parallel to the NW axis, as obtained for TO_l [Fig. 5(c)], is actually expected for an E_2 wurtzite Raman tensor, which results in exclusively perpendicular scattering [see Fig. 5(g)]. Thus, within the fitting and experimental errors, this polarization dependence clearly assigns the TO_l to the E_2^H mode. The TO_{ll} most probably corresponds to a wurtzite B_1^H mode. Though modes with B_1 symmetry are expected to be Raman silent, they can, however, be activated by disorder, following A_1 symmetry,[14] as we observe here.

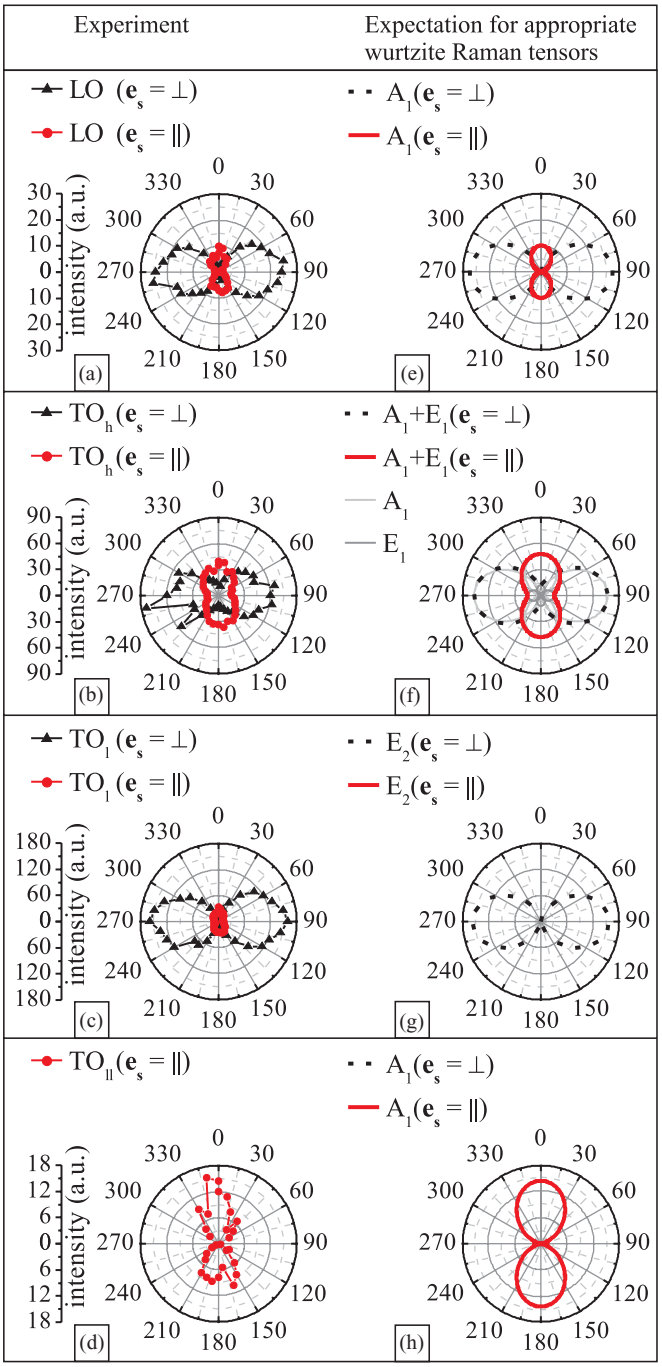

FIG. 5. (Color online) (a)–(d) Azimuthal dependence of the Raman scattering intensity for the four individual peaks observable for the InAs nanowires. (e)–(h) Polar behavior calculated by wurtzite-type Raman tensors with appropriate symmetry and parameters.

Furthermore, a comparison of the intensities of the single modes reveals that the E_2^H mode is strongly dominating the spectra for the 514.5-nm laser line, which is why all of our studies without polarization selection at this wavelength seem to exhibit a downshifted TO. The clear dominance of

wurtzite-type behavior in the mixed lattice structure is apparently due to resonant Raman scattering effects. A detailed mode-dependent resonant Raman study on these InAs NWs is currently under investigation.

V. SUMMARY

The Raman measurements on InAs NWs with stacking variations and WZ/ZB content have shown that the spectra exhibit several new features, most striking an apparent downshifted TO. A comparison of spectra taken under the four main scattering geometries revealed, that there are four phonon modes contributing to optical phonon scattering in these NWs. They correspond in frequency well to the InAs zincblende TO and LO modes at the Γ and L points, which is expected for wurtzite InAs. By recording the full azimuthal dependence of the Raman scattering intensity, it could be shown that the individual symmetry behavior of these new modes corresponds indeed to WZ-type phonons. Disorder-induced effects are mainly seen in the activation of the LO and B_1^H modes, as well as the rather large FWHM of the TO and E_2^H.

ACKNOWLEDGMENTS

The authors thank M. Bichler and H. Riedl for excellent experimental help. This research was supported financially by the DFG via the excellence cluster Nanosystems Initiative Munich (NIM), the SFB 631, the Institute for Advanced Study (IAS) of the TU München, and the Marie Curie FP7 Reintegration Grant.

[1] X. Duan, Y. Huang, R. Agarwal, and C. M. Lieber, Nature (London) **421**, 241 (2003).
[2] Y. Huang, X. Duan, and C. M. Lieber, Small **1**, 142 (2005).
[3] A. Ponzoni, E. Comini, G. Sberveglieri, J. Zhou, S. Z. Deng, N. S. Xu, Y. Ding, and Z. L. Wang, Appl. Phys. Lett. **88**, 203101 (2006).
[4] B. Tian, X. Zheng, T. J. Kempa, Y. Fang, N. Yu, G. Yu, J. Huang, and C. M. Lieber, Nature (London) **449**, 885 (2007).
[5] A. I. Boukai, Y. Bunimovich, J. Tahir-Kheli, J.-K. Yu, W. A. Goddard III, and J. R. Heath, Nature (London) **451**, 168 (2008).
[6] K. Tomioka, J. Motohisa, S. Hara, and T. Fukui, Nano Lett. **8**, 3475 (2008).
[7] A. L. Roest, M. A. Verheijen, O. Wunnicke, S. Serafin, H. Wondergem, and E. P. A. M. Bakkers, Nanotechnology **17**, S271 (2006).
[8] G. Koblmüller, S. Hertenberger, K. Vizbaras, M. Bichler, F. Bao, J.-P. Zhang, and G. Abstreiter, Nanotechnology **21**, 365602 (2010).
[9] S. Hertenberger, D. Rudolph, M. Bichler, J. J. Finley, G. Abstreiter, and G. Koblmüller, J. Appl. Phys. **108**, 114316 (2010).
[10] F. Glas, Phys. Rev. B **74**, 121302 (2006).
[11] R. E. Algra, M. A. Verheijen, M. T. Borgstrom, L.-F. Feiner, G. Immink, W. J. P. van Enckevort, E. Vlieg, and E. P. A. M. Bakkers, Nature (London) **456**, 369 (2008).
[12] K. A. Dick, P. Caroff, J. Bolinsson, M. E. Messing, J. Johansson, K. Deppert, L. R. Wallenberg, and L. Samuelson, Semicond. Sci. Technol. **25**, 024009 (2010).
[13] Y. F. Hsu *et al.*, Adv. Funct. Mater. **18**, 1020 (2008).
[14] M. Cardona and G. Güntherodt (eds.), *Light Scattering in Solids II: Basic Concepts and Instrumentation* (Springer-Verlag, Berlin, 1982).
[15] S. Piscanec, M. Cantoro, A. C. Ferrari, J. A. Zapien, Y. Lifshitz, S. T. Lee, S. Hofmann, and J. Robertson, Phys. Rev. B **68**, 241312 (2003).
[16] S. Yazji, I. Zardo, M. Soini, P. Postorino, A. F. i Morral, and G. Abstreiter, Nanotechnology **22**, 325701 (2011).
[17] K. Adu, Q. Xiong, H. Gutierrez, G. Chen, and P. Eklund, Appl. Phys. A **85**, 287 (2006).
[18] I. H. Campbell and P. M. Fauchet, Solid State Commun. **58**, 739 (1986).
[19] Y. Xiang, I. Zardo, L. Y. Cao, T. Garma, M. Hei, J. R. Morante, J. Arbiol, M. L. Brongersma, and A. F. i Morral, Nanotechnology **21**, 105703 (2010).
[20] G. Chen, J. Wu, Q. Lu, H. R. Gutierrez, Q. Xiong, M. E. Pellen, J. S. Petko, D. H. Werner, and P. C. Eklund, Nano Lett. **8**, 1341 (2008).
[21] I. Zardo, S. Conesa-Boj, F. Peiro, J. R. Morante, J. Arbiol, E. Uccelli, G. Abstreiter, and A. Fontcuberta i Morral, Phys. Rev. B **80**, 245324 (2009).
[22] J. Frechette and C. Carraro, Phys. Rev. B **74**, 161404 (2006).
[23] J. Wu, D. Zhang, Q. Lu, H. R. Gutierrez, and P. C. Eklund, Phys. Rev. B **81**, 165415 (2010).
[24] N. Begum, M. Piccin, F. Jabeen, G. Bais, S. Rubini, F. Martelli, and A. S. Bhatti, J. Appl. Phys. **104**, 104311 (2008).
[25] N. Begum, A. S. Bhatti, F. Jabeen, S. Rubini, and F. Martelli, J. Appl. Phys. **106**, 114317 (2009).
[26] D. Spirkoska *et al.*, Phys. Rev. B **80**, 245325 (2009).
[27] F. J. Lopez, E. R. Hemesath, and L. J. Lauhon, Nano Lett. **9**, 2774 (2009).
[28] S. Hertenberger, D. Rudolph, S. Bolte, M. Döblinger, M. Bichler, D. Spirkoska, J. J. Finley, G. Abstreiter, and G. Koblmüller, Appl. Phys. Lett. **98**, 123114 (2011).
[29] D. Kriegner*et al.*, Nano Lett. **11**, 1483 (2011).
[30] R. Carles, N. Saint-Cricq, J. B. Renucci, M. A. Renucci, and A. Zwick, Phys. Rev. B **22**, 4804 (1980).
[31] H. Harima, J. Phys. Condens. Matter **14**, R967 (2002).
[32] F. Zhou *et al.*, Phys. Rev. B **83**, 205416 (2011).
[33] R. Loudon, Adv. Phys. **13**, 423 (1964).
[34] J. F. Nye, *Physical Properties of Crystals: Their Representation by Tensors and Matrices* (Clarendon, Oxford, 1957).
[35] C. A. Arguello, D. L. Rousseau, and S. P. S. Porto, Phys. Rev. **181**, 1351 (1969).
[36] Z. V. Popović, M. Cardona, E. Richter, D. Strauch, L. Tapfer, and K. Ploog, Phys. Rev. B **41**, 5904 (1990).
[37] H. Richter, Z. P. Wang, and L. Ley, Solid State Commun. **39**, 625 (1981).
[38] S. Nakashima, H. Ohta, M. Hangyo, and B. Palosz, Philos. Mag. B **70**, 971 (1994).

[39]S. Nakashima, K. Kisoda, H. Niizuma, and H. Harima, Physica B: Condensed Matter **219-220**, 371 (1996).
[40]S. Rohmfeld, M. Hundhausen, and L. Ley, Phys. Rev. B **58**, 9858 (1998).
[41]M. Soini, I. Zardo, E. Uccelli, S. Funk, G. Koblmüller, A. F. i Morral, and G. Abstreiter, Appl. Phys. Lett. **97**, 263107 (2010).
[42]M. Cantoro *et al*., Phys. Status Solidi A **208**, 129 (2011).
[43]L. Cao, L. Laim, P. D. Valenzuela, B. Nabet, and J. E. Spanier, J. Raman Spectrosc. **38**, 697 (2007).
[44]A. F. Oskooi, D. Roundy, M. Ibanescu, P. Bermel, J. D. Joannopoulos, and S. G. Johnson, Comput. Phys. Commun. **181**, 687 (2010).
[45]D. E. Aspnes and A. A. Studna, Phys. Rev. B **27**, 985 (1983).
[46]R. Carles, N. Saint-Cricq, J. B. Renucci, A. Zwick, and M. A. Renucci, Phys. Rev. B **22**, 6120 (1980).
[47]M. Möller, M. M. de Lima, A. Cantarero, L. C. O. Dacal, J. R. Madureira, F. Iikawa, T. Chiaramonte, and M. A. Cotta, Phys. Rev. B **84**, 085318 (2011).